Color transparency and Dirac-based spin effects in $(e, e'p)$ reactions

W. R. Greenberg* and G. A. Miller
Department of Physics, FM-15, University of Washington, Seattle, Washington 98195
(Received 16 September 1993; revised manuscript received 20 December 1993)

Color transparency (CT) in high momentum transfer $(e, e'p)$ and $(e, e'\vec{p})$ reactions is explored. The vector nature of the photon and the spin of the proton and photon are treated explicitly by describing the initial bound proton and the ejected wave packet as four-component Dirac spinors. Such effects, ignored in previous calculations, yield several results: (1) The use of Dirac-based optical potentials in the "standard calculation" (ignoring CT) leads to smaller cross sections than predicted before. (2) The normal component of the ejectile polarization, which vanishes in the limit of full CT, is found to approach zero very slowly as the energy increases. (3) Due to the presence of the $1H_{11/2}$ orbital, a measurement of the normal-transverse response in ^{208}Pb could afford the opportunity to see CT at quite low momentum transfers ~ 1 GeV/c. (4) The four-component nature of our formalism allows us to determine that our calculations are roughly consistent with current conservation, except when the momentum of the struck nucleon is greater than about 150 MeV/c.

PACS number(s): 12.38.Aw, 13.60.−r, 13.85.−t, 24.85.+p

I. INTRODUCTION

Color transparency (CT) is the postulated [1,2] absence of final- (or initial-) state interactions caused by the cancellation of color fields of a system of quarks and gluons with small spatial separation. For example, suppose an electron impinges on a nucleus knocking out a proton at high momentum transfer. The consequence of color transparency is that there is no exponential loss of flux as the ejected particle propagates through the nucleus. We restrict our attention to processes for which the fundamental reaction is quasielastic. This requires that the nuclear excitation energy be known well enough to ensure that no extra pions are created. This subject is under active experimental investigation [3–7].

The existence of color transparency depends on (1) the formation of a small-sized wave packet in a high momentum transfer reaction, (2) the interaction between such a small object and nucleons being suppressed (color neutrality or screening), and (3) the wave packet escaping the nucleus while still small. That color neutrality (screening) causes the cross section of small-sized color singlet configurations with hadrons to be small was found in Refs. [8], and is reviewed in Refs. [9,10]. So we take item (2) as given. The truth of item (1), for subasymptotic energies, is an interesting issue, see Refs. [10–12]. Here we shall be concerned with testing the assumption that (1) holds.

It is reasonable to expect that the small object expands as it moves through the nucleus [13,14]. For present experiments [3–7] concerned with the onset of color transparency, the value of transferred momentum Q^2 is increased from a low value, where the expansion is rapid. Thus the final-state interactions are suppressed but not zero.

This paper is concerned with the quasielastic $(e, e'p)$ reaction scattering for Q^2 starting at about 1 GeV$^2/c^2$, where the conventional distorted wave impulse approximation (DWIA) is known to be valid, up to values of about 10–20 GeV$^2/c^2$. The published calculations of color transparency effects in this range seem to treat the photon as a scalar object and ignore the spin of the outgoing proton. Thus we use the full Lorentz structure of the matrix element for the electroproduction of nucleons from nuclei. What do we hope to gain by introducing this complication? It is necessary to check that predictions with the new formalism are not much different than previous ones. Furthermore, the normal component of the polarization of the ejected proton [in $(e, e'\vec{p})$ experiments] vanishes in the limit where final-state interactions are absent [15]. Therefore, the spin-dependent observables may provide a very sensitive measure of the effects of CT. Most importantly, an experiment has been proposed and approved, to be run at CEBAF [7], which will measure the energy dependence of the unpolarized cross section and the normal component of the ejected proton's polarization. It is desirable to have theoretical predictions ready to be confronted by the experimental results.

In a previous paper [16] a multiple-scattering series for the interaction between the outgoing wave packet and the nucleus was developed within the framework of Glauber (eikonal) theory. The effects of CT were included by treating the outgoing wave packet as a linear superposition of baryonic states. The present approach has the same philosophy, but four-component Dirac spinors are used for the scattering- and bound-state wave functions.

At medium energies, where there is no color transparency, this "Dirac phenomenology" has been successfully applied to proton-nucleus interactions [17,18] and quasielastic $(e, e'p)$ reactions. In particular, the proton-

*Present address: Department of Physics, University of Pennsylvania, Philadelphia, PA 19104.

nucleus analyzing powers, spin rotation functions, and differential cross sections were successfully described. Furthermore, Do Dang and Van Gai [19] showed that this phenomenology may account for the suppression of the longitudinal response function relative to the transverse response observed in the $(e, e'p)$ reaction. Apart from effects of the composite nature of the nucleon, such as CT, the (Dirac) impulse approximation should be even better for the higher energies of interest here.

The organization of this paper is as follows. In Sec. II we display standard formulas for the $(e, e'\vec{p})$ cross section and polarization in terms of the nuclear current matrix element (NCME). This defines our notation. In Sec. III, the NCME is computed using the Dirac impulse approximation. Section III is generalized to include the effects of CT by treating the outgoing wave packet as a linear superposition of (four-component) baryonic states in Sec. IV. The approximation schemes of Ref. [16] are used to evaluate the CT wave functions in Sec. V. In Sec. VI we present numerical results for total cross section ratios, differential unpolarized cross sections, differential normal polarizations, individual nuclear response functions, current conservation violations, Fermi motion, and the effects of the purely relativistic lower components. Section VII contains a summary and some concluding comments.

We make no attempt to accurately include the effects of short-range nucleon-nucleon correlations. The estimates of the size of this effect range from about zero [20] to 50% [21]. In any case, the correlations are a property of the nuclear ground state so the effects are expected to be independent of energy in the kinematic regime of our interest. Therefore, we take the point of view that while correlations may affect the overall magnitude of our ratios, the Q^2 dependence of the observables is well modeled by our formalism. We also neglect the possibility that the nucleon properties are much modified in medium. A recent analysis of the Brookhaven National Laboratory (BNL) (p, pp) experiment argues that the hard proton-proton scattering may be reduced by a factor of 2 due to the effects of the nuclear medium [22]. If so, the nucleon form factor could also be modified in a similar way. Indeed, that very point is argued in Ref. [23] where 10–15 % effects are found. At present it is difficult to understand the precise origin and size of such effects, so we neglect them. We also make no attempt to completely review the CT literature.

The details and final results of the SLAC experiment [6] are not now available, and it is important to use the precise experimental acceptance in computing observables. Thus we leave a detailed assessment of that experiment to a future publication.

II. THE NUCLEAR CURRENT MATRIX ELEMENT AND CROSS SECTION

We describe the spin-dependent formalism to make clear the definitions and conventions [24] used in this paper. Consider the $(e, e'\vec{p})$ process of bombarding a spin-0 nucleus with unpolarized electrons and detecting the polarization of the knocked out protons. The kinematics

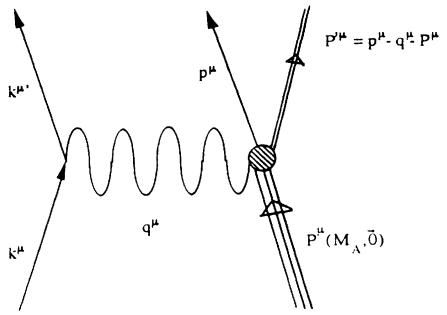

FIG. 1. Coordinate system used to describe the $(\vec{e}, e'\vec{N})$ reaction.

are displayed in Fig. 1. We take the virtual photon to lie along the $\check{\mathbf{Z}}$ direction, and the electron scattering plane to be the Y-Z plane. The rest-frame polarization of the outgoing proton is taken as along a direction $\check{\mathbf{s}}_R$. We use the notation that $\check{\mathbf{a}}$ describes a unit vector in the direction of $\mathbf{a}$. The upsidedown "hat" is used to distinguish unit vectors from operators.

The scattering amplitude is defined as usual as

$$M_{\alpha,\check{\mathbf{s}}_R} = j_\mu J^\mu_{\alpha,\check{\mathbf{s}}_R}, \tag{2.1}$$

where j_μ is the matrix element of the electron current and $J^\mu_{\alpha,\check{\mathbf{s}}_R}$ is the matrix element of the nuclear current (NCME); it depends on the rest-frame spin projection $\check{\mathbf{s}}_R$ of the ejected proton. The sum is over all occupied shells.

Since the electron current is well known (see, e.g., Ref. [24]), the crucial quantity is the nuclear current matrix element (NCME). We use the one-photon-exchange approximation and the nuclear shell model to evaluate the NCME:

$$J^\mu_{\alpha,\check{\mathbf{s}}_R}(q) = \langle \alpha | T^{\mu\dagger}_H(q) | \Psi_{\mathbf{p},-\check{\mathbf{s}}_R} \rangle^{(+)}, \tag{2.2}$$

where q is the four-vector of the virtual photon, and can be determined solely from the electron kinematics. The initial state of this knockout process is labeled by the shell model state of a bound proton, α. The binding energy of the nucleon in shell α is small compared with the other energy scales in the problem and is neglected. In the final state, a proton moves with a momentum $\mathbf{p}$, energy $E_p = \sqrt{\mathbf{p}^2 + M_N^2}$, and with rest-frame spin projection $\check{\mathbf{s}}_R$; M_N is the nucleon mass. The residual nucleus is an α-hole state, which is not detected, but which is assumed to recoil with negligible kinetic energy. The initial and final states are connected by a vector operator denoted as $T^\mu_H(q)$ which describes the absorption of a virtual photon on a proton in the nucleus. The overlap of the initial and final nuclear states is imagined to be a single-particle state of a nucleon bound in shell model state α.

Saha and collaborators [7] plan on measuring the differential cross section and the normal component (to the photonuclear scattering plane) of the proton polarization. The differential cross section is given by

$$\frac{d^3\sigma}{d\epsilon_{k'}d\Omega_{k'}d\Omega_p} = \frac{M_N|\mathbf{p}|}{2(2\pi)^3}\left(\frac{d\sigma}{d\Omega_{k'}}\right)_{\rm Mott} \times \sum_\alpha \left[|M_{\alpha,\check{\mathbf{s}}_R}|^2 + |M_{\alpha,-\check{\mathbf{s}}_R}|^2\right], \quad (2.3)$$

where the sum is over all occupied shells, α. The solid angle $d\Omega_p = \sin\zeta\, d\zeta\, d\beta$ refers to the ejected proton, while the solid angle $d\Omega_{k'}$ refers to the scattered electron. The precise direction of the spin, here, does not matter as it is summed over. It is also useful to consider the "total" cross section, obtained by integrating over the solid angle of the outgoing proton. This is very similar to the observables measured in Ref. [6]. More details are provided in Ref. [24].

The normal component of the polarization vector is defined as

$$P_n = \left(\frac{d^3\sigma}{d\epsilon_{k'}d\Omega_{k'}d\Omega_p}\right)^{-1}\frac{M_N|\mathbf{p}|}{2(2\pi)^3}\left(\frac{d\sigma}{d\Omega_{k'}}\right)_{\rm Mott} \times \sum_\alpha \left[|M_{\alpha,\check{\mathbf{n}}}|^2 - |M_{\alpha,-\check{\mathbf{n}}}|^2\right], \quad (2.4)$$

where the spin of the ejected proton is projected along $\check{\mathbf{n}} = \frac{\mathbf{q}\times\mathbf{p}}{|\mathbf{q}\times\mathbf{p}|}$, which is normal to the photonuclear scattering plane. For in-plane scattering, this is only component of the polarization which is nonvanishing. Again, the sum on α is over all occupied shells. The normal-transverse response function R_T^n is of special interest here. This is obtained from (2.4) by keeping only the contributions of the transverse components of the current, $J^{\mu=1,2}_{\alpha,\check{\mathbf{s}}_R}(q)$, to $M_{\alpha,\check{\mathbf{n}}}$ that appears in the sum over α.

III. DWIA FORMALISM

The DWIA approximation to the matrix element of Eq. (2.2) is specified by defining the single-particle bound-state wave function, the electromagnetic current operator, and the scattering wave function. We discuss each of these.

A. Bound state

In earlier work, the ejected proton was taken as initially bound in a nonrelativistic one-particle shell model state. Since the present formalism is spin dependent and relativistic, it is necessary to look for a relativistic single-particle shell model state which is a four-component Dirac spinor. Here we use the finite nucleus mean field model of Horowitz and Serot [25], which is an approximation to a quantum hadrodynamics (QHD) Lagrangian. Our opinion is that QHD is not a fundamental field theory. However, its mean field approximation yields realistic nuclear densities and four-component bound-state wave functions.

B. Current operator

The vector current operator represents the absorption of a virtual photon by a nucleon bound in a nucleus. Because this nucleon is somewhat off the energy shell, the current operator, in general, can be expressed in terms of scalar functions of the four-momenta multiplied by any of 12 four-vectors [24]. Since the bound nucleon is only slightly off shell (the binding energy is small), and any other choice is only a guess, the current operator is chosen to be that of the free nucleon. Thus, we define the configuration-space matrix elements, which are matrices in the Dirac space, as

$$\langle\mathbf{R}|T_H^\mu(q)|\mathbf{R}'\rangle = e^{i\mathbf{q}\cdot\mathbf{R}}\delta^3(\mathbf{R}-\mathbf{R}')\,\gamma^0\Gamma^\mu(q), \quad (3.1)$$

where

$$\Gamma^\mu(q) = F_1(q^2)\gamma^\mu + \frac{i}{2M_N}F_2(q^2)\sigma^{\mu\nu}q_\nu, \quad (3.2)$$

and $F_1(q^2)$ and $F_2(q^2)$ are the usual Dirac and Pauli form factors of the nucleon. We use the well-known dipole parametrization for the electric and magnetic form factors, $G_E(q^2)$ and $G_M(q^2)$. Note that the γ^0 of Eq. (3.1) enters to convert the standard $u^\dagger$ into a $\bar{u}$.

C. Optical potential and distorted wave

We have chosen the bound-state proton wave function to be a relativistic four-component object, and the current operator to be a 4 × 4 matrix. Thus the proton wave is also chosen as a Dirac spinor, obtained by solving a suitable one-particle wave equation.

Treating the Dirac equation as a one-particle equation is problematic. However, the difficulties can be identified (see, e.g., Sec. 2 of Ref. [26].) Here we are interested in the scattering energy eigenstates of an interacting Dirac Hamiltonian. Such eigenstates propagate with no transitions to the negative energy states, so interpreting the Dirac equation as a governing equation of a single-particle relativistic quantum mechanics is allowed. We stress that we are using the Dirac impuluse equation as a phenomenological tool, which is consistent with much medium energy data. At higher energies the impulse approximation is expected to be even better.

The complex potentials that appear in the Dirac equation are a Lorentz scalar V_s and a time component of a four-vector, V_v. In the relativistic (forward scattering) impulse approximation, the scalar and vector optical potentials, V_s and V_v, are proportional to forward Dirac scalar and Dirac vector scattering amplitudes (F_s^0, F_v^0) and to the scalar and vector nuclear densities [18,27] (ρ_s, ρ_v), such that

$$V_s(\mathbf{R}) = r\,F_s^0\rho_s(\mathbf{R}) \quad \text{and} \quad V_v(\mathbf{R}) = r\,F_v^0\rho_v(\mathbf{R}), \quad (3.3)$$

and $r = -4\pi i p_{\rm lab}/M_N$ is a kinematical factor. The quantities $\rho_s(R)$ and $\rho_v(R)$ are those of the QHD mean field model discussed above. The ranges of the interactions are taken as small compared to the nuclear size and are neglected.

The quantities F_s^0 and F_v^0 are obtained from NN scattering data [28–31]. The Appendix shows how we determine the values of F_s^0 and F_v^0. Since the strengths

depend on the energy-dependent NN scattering data, we consider our calculations reliable only at the energies where sufficient data exist to determine F_s^0 and F_v^0. The results are displayed in Table I. It is useful, when examining the table, to recall that $M_N V_s(\mathbf{R}) + E V_v(\mathbf{R})$, where $E = \sqrt{p^2 + M_N^2}$, enters in the Dirac equation. Thus at high energies the vector potential is the important quantity and the optical potentials of Table I are as absorptive as the usual optical potentials. The last two columns of Table I show the potential strengths in MeV, where we use $\rho_0 = 0.166$ fm^{-3}. We also note that each of $V_s(\mathbf{R})$ and $V_s(\mathbf{R})$ have a significant real part, even when the real part of the forward scattering amplitude is small.

The Dirac equation for the distorted wave is given by

$$H\Psi^{(+)}_{\mathbf{p},\check{\mathbf{s}}_R}(\mathbf{R}) = \Big[-i\boldsymbol{\alpha}\cdot\boldsymbol{\nabla} + \beta\,[M_N + V_s(R)] + V_v(R)\Big]\Psi^{(+)}_{\mathbf{p},\check{\mathbf{s}}_R}(\mathbf{R}) = E\Psi^{(+)}_{\mathbf{p},\check{\mathbf{s}}_R}(\mathbf{R}). \quad (3.4)$$

This equation is solved by separation into two coupled first-order differential equations. The eikonal form of the solution to this equation is well known [32] and is given by

$$\Psi^{(+)}_{\mathbf{p},-\check{\mathbf{s}}_R}(\mathbf{R}) = \mathcal{N}\begin{pmatrix} 1 \\ \frac{-i\boldsymbol{\sigma}\cdot\boldsymbol{\nabla}}{E+M_N+V_s(R)-V_v(R)} \end{pmatrix} e^{ipZ} \times \exp\left[\int_{-\infty}^{Z} dZ'\Omega(\mathbf{B},Z')\right]\chi_{-\check{\mathbf{s}}_R}, \quad (3.5)$$

where $\mathbf{R} \equiv \mathbf{B} + Z\check{\mathbf{Z}}$,

$$\Omega(\mathbf{B},Z') = \frac{1}{2ip}\Big\{U_c(\mathbf{B},Z') + U_{\rm so}(\mathbf{B},Z')\,[\boldsymbol{\sigma}\cdot\mathbf{B}\times\mathbf{p} - ipZ']\Big\}, \quad (3.6)$$

$\mathbf{R}\cdot\mathbf{p} = pZ$, and $\mathbf{B}\cdot\mathbf{p} = 0$. Also note that we have used outgoing boundary conditions and changed the sign of the rest-frame spin projection, as in Eq. (2.2). The normalization is $\mathcal{N} = \sqrt{(E+M_N)/(2M_N)}$. The Dirac scalar and vector potentials have been eliminated in favor of new central (U_c) and spin-orbit ($U_{\rm so}$) potentials:

$$U_c(R) = 2EV_v(R) + 2M_N V_s(R) + V_s^2(R) - V_v^2(R), \quad (3.7)$$

$$U_{\rm so}(R) = \frac{1}{E + M_N + V_s(R) - V_v(R)} \times \frac{1}{R}\frac{\partial}{\partial R}\{V_v(R) - V_s(R)\}. \quad (3.8)$$

Finally, we note one other complication. The eikonal wave function presented in Eq. (3.5) takes the particle to travel along the $\check{\mathbf{Z}}$ axis (direction of the virtual photon). At very high energies, the difference between $\check{\mathbf{p}}$ and $\check{\mathbf{Z}}$ is small and should be inconsequential. However, assuming that $\check{\mathbf{p}} = \check{\mathbf{Z}}$ leads to the result that the response function R_{TT} vanishes. But R_{TT} is not zero, as can be checked by considering the plane-wave limit. Thus we account for the difference between $\check{\mathbf{p}}$ and $\check{\mathbf{Z}}$ in our calculations. See Ref. [33] for details.

IV. COLOR TRANSPARENCY

Color transparency occurs in the $(e,e'p)$ reaction when a small-sized wave packet, produced by the absorption of a photon, leaves the nucleus without interacting. Our approach to including CT is to treat the outgoing wave packet as a linear superposition of baryonic states.

The CT scattering matrix element with spin along $\check{\mathbf{s}}_R$ $\mathcal{M}_{\alpha,\check{\mathbf{s}}_R}$ is given by

$$\mathcal{M}_{\alpha,\check{\mathbf{s}}_R} = j_\mu \mathcal{J}^\mu_{\alpha,\check{\mathbf{s}}_R}\,, \quad (4.1)$$

where $\mathcal{J}^\mu_{\alpha,\check{\mathbf{s}}_R}$ is the nuclear current matrix element including the effects of CT. The triple differential cross section is given by Eq. (2.3), with the replacement of $M_{\alpha,\check{\mathbf{s}}_R}$ by $\mathcal{M}_{\alpha,\check{\mathbf{s}}_R}$. Similarly, the polarization including CT is given by Eq. (2.4) with the same replacement. Let us now compute $\mathcal{J}^\mu_{\alpha,\check{\mathbf{s}}_R}$. We follow the method in Ref. [16] and write

$$\mathcal{J}^\mu_{\alpha,\check{\mathbf{s}}_R}(q) = \langle N,\alpha|\widehat{T}^{\mu\dagger}_H(q)|\Psi_{N,\mathbf{p},-\check{\mathbf{s}}_R}\rangle^{(+)}\,. \quad (4.2)$$

Here, $|\Psi_{N,\mathbf{p},-\check{\mathbf{s}}_R}\rangle^{(+)}$ is a column vector representing a linear superposition of baryons, with each element depending on the nuclear coordinate $\mathbf{R}$. The subscript on Ψ denotes the boundary condition that ultimately a nucleon N moving with momentum $\mathbf{p}$ and rest-frame spin along $-\check{\mathbf{s}}_R$ is detected. The overlap of this state

TABLE I. Energy-dependent strengths of optical potentials. Q^2 is in GeV^2 and $p_{\rm lab}$ is in GeV. $r = -4\pi i p_{\rm lab}/M_N$.

Q^2	$p_{\rm lab}$	$r\,F_s^0$ (fm^2)	$r\,F_v^0$ (fm^2)	$\rho_0\,r\,F_s^0$ (MeV)	$\rho_0\,r\,F_v^0$ (MeV)
0.96	1.1	$-9.566+1.768i$	$5.720-2.291i$	$-313.3+57.91i$	$187.4-75.05i$
1.88	1.7	$-9.550+3.748i$	$4.970-3.895i$	$-312.8+122.8i$	$162.8-127.6i$
2.38	2.0	$-10.46+4.219i$	$4.912-3.936i$	$-342.6+138.2i$	$160.9-128.9i$
3.25	2.5	$-7.243+4.047i$	$3.396-3.573i$	$-237.3+132.6i$	$111.2-117.0i$
4.14	3.0	$-10.75+6.735i$	$3.836-4.124i$	$-352.0+220.6i$	$125.6-135.1i$
5.96	4.0	$-7.091+2.147i$	$2.155-2.540i$	$-232.3+70.33i$	$70.59-83.20i$
9.65	6.0	$-7.681+2.398i$	$1.831-2.380i$	$-251.6+78.56i$	$59.98-77.96i$
20.86	12.0	$-7.631+10.73i$	$1.168-2.809i$	$-250.0+351.4i$	$38.27-92.03i$

with the nuclear position state $\langle \mathbf{R}|$ gives a vector in the baryonic space, which we identify with boldface type: $\langle \mathbf{R}|\Psi_{N,\mathbf{p},-\check{\mathbf{s}}_R}\rangle^{(+)} = \mathbf{\Psi}^{(+)}_{N,\mathbf{p},-\check{\mathbf{s}}_R}(\mathbf{R})$. The operator $\widehat{T}^{\mu\dagger}_H(q)$ acts on the quarks; we shall evaluate its matrix elements in baryonic states. The state $\langle N,\alpha|$ is the same relativistic bound-state proton wave function as in the DWIA calculations, Eq. (4.2).

A. Current operator

Upon absorption of a high-energy photon, the proton is converted into a coherent superposition of an infinite number of baryon states (a wave packet). We label the individual components by a discrete quantum number, m, for simplicity of notation. Then, we identify the relevant inelastic transition Dirac and Pauli form factors by taking the matrix elements of the current operator to be

$$\langle N,\mathbf{R}|\widehat{T}^{\mu}_H(q)|m,\mathbf{R}'\rangle = e^{i\mathbf{q}\cdot\mathbf{R}}\delta^3(\mathbf{R}-\mathbf{R}')\,\gamma^0\Gamma^{\mu}_{N,m}(q), \tag{4.3}$$

where

$$\Gamma^{\mu}_{N,m}(q) = F_{1_{N,m}}(q^2)\gamma^{\mu} + \frac{i}{2M_N}F_{2_{N,m}}(q^2)\sigma^{\mu\nu}q_{\nu}. \tag{4.4}$$

Thus the ejectile is a coherent superposition of an infinite number of states m, with amplitude proportional to $\Gamma^{\mu}_{N,m}(q)$. These amplitudes can be related to deep inelastic structure functions [34]. A comparison between the present method and that of Ref. [34] is given in Sec. V A.

B. Optical potential

We now consider the optical potentials $V_s(R)$ and $V_v(R)$ which represent the interaction between the wave packet and the nucleus. These optical potentials are essentially products of the baryon-nucleon scattering amplitude operator $f_{s(v)}(\widehat{b}^2)$ with $\rho_{s(v)}$. At present, there is no detailed knowledge about the precise form for $f_{s(v)}(\widehat{b}^2)$. However, some general properties are known. For small wave packets with $b^2 \ll b_H^2$ with $b_H^2 \equiv \langle N|\widehat{b}^2|N\rangle$, $f_{s(v)}$ should vanish. Interactions do occur for larger wave packets. For nonzero but still small-sized wave packets, the interaction goes like

$$\lim_{\widehat{b}^2\to 0} f_{s(v)}(\widehat{b}^2) \to \frac{\widehat{b}^2}{b_H^2}. \tag{4.5}$$

The operators $f_{s(v)}$ are normalized such that

$$f_{s(v)}(\widehat{b}^2 = 0) = 0, \tag{4.6}$$

$$\langle N|f_{s(v)}(\widehat{b}^2)|N\rangle = 1. \tag{4.7}$$

The matrix elements of the scalar and vector operators can then be written as

$$\langle m,\mathbf{R}|\widehat{V}_{s(v)}|m',\mathbf{R}'\rangle = \delta^3(\mathbf{R}-\mathbf{R}')V_{s(v)}(\mathbf{R}) \times\langle m|f_{s(v)}(\widehat{b}^2)|m'\rangle. \tag{4.8}$$

To simplify the notation, we define the quantity $V_{s(v)}(\mathbf{R})f_{s(v)}(\widehat{b}^2) \equiv \widehat{V}_{s(v)}(\mathbf{R})$.

In practice, we use the same $f(\widehat{b}^2)$ for both the scalar and vector potentials: $f(\widehat{b}^2) = f_v(\widehat{b}^2) = f_s(\widehat{b}^2)$. There is no information available at present on possible differences. However, an explicit evaluation of the two-gluon exchange in perturbative QCD leads to a purely vector potential [35]. We have shown in Sec. III that the vector potential is also dominant in our phenomenology. Thus the results we present are not sensitive to the choice of $f_s(\widehat{b}^2)$ for the scalar potentials.

C. Distorted wave

In this section we obtain the wave equation for the propagation of the wave packet formed in the hard collision through the nucleus. Start by considering the time-independent Dirac equation. The equivalent Dirac Hamiltonian should now be considered an operator in the quark space. Thus the wave equation is

$$\begin{aligned}\widehat{H}\mathbf{\Psi}^{(+)}_{N,\mathbf{p},\check{\mathbf{s}}_R}(\mathbf{R}) &= \Big[-i\boldsymbol{\alpha}\cdot\boldsymbol{\nabla} + \beta\left(\widehat{M} + \widehat{V}_s(R)\right) \\ &\quad + \widehat{V}_v(R)\Big]\mathbf{\Psi}^{(+)}_{N,\mathbf{p},\check{\mathbf{s}}_R}(\mathbf{R}) \\ &= E\mathbf{\Psi}^{(+)}_{N,\mathbf{p},\check{\mathbf{s}}_R}(\mathbf{R}),\end{aligned} \tag{4.9}$$

where E is the energy and we have already taken the matrix element in the external configuration space. That is, $\mathbf{\Psi}^{(+)}_{N,\mathbf{p},\check{\mathbf{s}}_R}(\mathbf{R}) = \langle \mathbf{R}|\Psi_{N,\mathbf{p},\check{\mathbf{s}}_R}\rangle^{(+)}$. In this notation, $\widehat{M}^2$ is the baryon mass operator squared: $\widehat{M}^2|m\rangle = M_m^2|m\rangle$. The nucleon is the ground state with $m = N$ having eigenvalue M_N^2. The combination

$$\widehat{\mathbf{p}}^2 \equiv E^2 - \widehat{M}^2 \tag{4.10}$$

is also a quark space operator which can be interpreted as the baryon momentum operator squared. This operator accounts for the different kinematics with which the wave packet components propagate through the nucleus. Here $\widehat{\mathbf{p}}$ is also a three-vector in the $\check{\mathbf{Z}}$ direction; $\widehat{\mathbf{p}} = \widehat{p}\check{\mathbf{Z}}$.

The Dirac equation can again be solved by eliminating the lower components. Then we see that the CT scalar and vector Dirac potentials (which are operators in the internal space) can be eliminated in favor of combinations given by

$$\begin{aligned}\widehat{U}_c(R) &= 2E\widehat{V}_v(R) + \left\{\widehat{M},\widehat{V}_s(R)\right\} + \left[\widehat{M},\widehat{V}_v(R)\right] \\ &\quad + \widehat{V}_s^2(R) - \widehat{V}_v^2(R),\end{aligned} \tag{4.11}$$

$$\begin{aligned}\widehat{U}_{so}(R) &= \frac{1}{R}\left[\frac{\partial}{\partial R}\left(\widehat{V}_v(R) - \widehat{V}_s(R)\right)\right] \\ &\quad \times\left(E + \widehat{M} + \widehat{V}_s(R) - \widehat{V}_v(R)\right)^{-1},\end{aligned} \tag{4.12}$$

where the square (curly) brackets are the (anticommutator) commutator symbols. We also define "path-evolved" versions of the operators of Eqs. (4.11) and (4.12) as

$$\widehat{\mathcal{U}}_{c(\mathrm{so})}(\mathbf{R}) = e^{-i\widehat{p}Z}\widehat{U}_{c(\mathrm{so})}(R)e^{i\widehat{p}Z}. \tag{4.13}$$

We solve the Dirac equation in the eikonal approximation so that the solution to the resulting eikonal first-order equation is a path-ordered exponential. The notation is simplified by defining an operator $\widehat{\Omega}$ such that

$$\widehat{\Omega}(\mathbf{B}, Z') = \frac{1}{2i\widehat{p}}\Big[\widehat{\mathcal{U}}_c(\mathbf{B}, Z') + \widehat{\mathcal{U}}_{\mathrm{so}}(\mathbf{B}, Z')\,(\boldsymbol{\sigma}\cdot\mathbf{B}\times\widehat{\mathbf{p}} - i\widehat{p}Z')\Big]. \tag{4.14}$$

Note that $[\widehat{\Omega}(\mathbf{R}), \widehat{\Omega}(\mathbf{R}')] \neq 0$ since $\widehat{p}$ and $\widehat{b}$ do not commute. This is because $\widehat{p}$ contains $\widehat{M}^2$, and $[\widehat{M}^2, f(\widehat{b}^2)] \neq 0$.

We note that the eikonal approximation is valid when the potentials are small compared to the momentum p; terms of order V^2/p^2 are ignored. Thus we may make the replacement $[E + \widehat{M} + \widehat{V}_s(\mathbf{R}) - \widehat{V}_v(\mathbf{R})]^{-1} \approx [E + \widehat{M}]^{-1}$, in Eq. (4.12). In performing the calculations, one also encounters terms like p/p_{2m} and $(E + M_N)/(E + M_{2m})$. We set such terms to unity. The errors introduced by using these approximations are very small.

Next we use the wave function of Eq. (4.9) to write the NCME of Eq. (4.2) as

$$\mathcal{J}^{\mu}_{\alpha,\check{\mathbf{s}}_R}(q) = \int d^3R\,\overline{\Phi}_{\alpha}(\mathbf{R})\,e^{-i\mathbf{q}\cdot\mathbf{R}} \times \sum_m \Gamma^{\mu}_{N,m}(q)\,\Psi^{(+)}_{\mathrm{CT},\mathbf{p},-\check{\mathbf{s}}_R}(\mathbf{R}, m)\ , \tag{4.15}$$

where $\overline{\Gamma}^{\mu} = \gamma^0\,[\Gamma^{\mu}]^{\dagger}\,\gamma^0$; the nucleon current operator is defined in Eq. (3.1). The quantity $\Psi^{(+)}_{\mathrm{CT},\mathbf{p},-\check{\mathbf{s}}_R}(\mathbf{R}, m)$ is mth component of the outgoing state such that

$$\Psi^{(+)}_{\mathrm{CT},\mathbf{p},-\check{\mathbf{s}}_R}(\mathbf{R}, m) = \mathcal{N}\langle m|\begin{pmatrix} 1 \\ \frac{-i\boldsymbol{\sigma}\cdot\boldsymbol{\nabla}}{E+\widehat{M}+\widehat{V}_s(\mathbf{R})-\widehat{V}_v(\mathbf{R})} \end{pmatrix} e^{i\widehat{p}Z}\mathcal{P}\exp\left[\int_{-\infty}^{Z} dZ'\,\widehat{\Omega}(\mathbf{B}, Z')\right]|N\rangle\chi_{-\check{\mathbf{s}}_R}, \tag{4.16}$$

where we have taken the momentum of the outgoing wave packet to lie along the $\check{\mathbf{Z}}$ direction in Eq. (4.16) but not in the calculations. Above, $\mathcal{P}$ is the path-ordering symbol. The effects of CT effects can be seen by comparing this expression with Eq. (3.5). We have projected the column vector $\boldsymbol{\Psi}$ on to the nucleon state to be detected, and could also project on to a nucleonic isobar to obtain the isobar production amplitude. The inelastic nucleon current operator, $\Gamma^{\mu}_{N,m}$, is defined in Eq. (4.4).

The expression for the CT wave function, shown in Eq. (4.16), is the central formal result of this paper.

At this stage, we may proceed to make the expansions and approximations, as in Ref. [16], which allow a numerical evaluation of the CT wave function, Eq. (4.16), the NCME, Eq. (4.15), and ultimately of the $(e, e'\vec{p})$ cross section and polarization. The definitions of these approximations are only slight generalizations of those in Ref. [16]. We find that neglecting the path ordering is a good approximation; see Ref. [33].

V. MODELS

The formalism described above can be used to compute color transparency effects for any choice of baryon spectrum and function $f(\widehat{b}^2)$. An earlier calculation [34] showed how such choices could be avoided by treating the expansion of the wave packet in terms of measured diffractive dissociation and deep inelastic scattering cross sections. But the spin dependence was not extracted in Ref. [34]. Thus we must model the spectrum and interaction.

A. Wave-packet–nucleon interaction and quark space

To proceed further we need specific forms for $\widehat{f}$ and the states $|m\rangle$. We choose the interaction to be

$$f(\widehat{b}^2) = \widehat{b}^2/b_H^2, \tag{5.1}$$

as in Eq. (4.5). Further, we choose the internal baryonic states to be described by the full spectrum of a two-dimensional transverse harmonic oscillator. For interactions of the form $f(\widehat{b}^2)$, the use of three-dimensional oscillators leads to the same results as those of the two-dimensional case. We calculate transparencies for $b_H = 1\,fm$ and for two different values of the oscillator spacing: $M_2^2 - M_N^2 = 1.19\,\mathrm{GeV}^2$ and $M_2^2 - M_N^2 = 2.36\,\mathrm{GeV}^2$. These simple choices reasonably represent the present (lack of detailed) knowledge of $f(\widehat{b}^2)$ and the baryon wave functions.

One may compare the present model with that of Ref. [34]. The first step is to compare the results of Ref. [34] with earlier work using the harmonic oscillator basis [14]. This shows that the present model for expansion corresponds to using the realistic inputs if one employs the low value of M_2^2 for Q^2 smaller than about 5 GeV^2 and the high value of M_2^2 for larger values of Q^2. This is if one uses the "power law" form of Ref. [34]. The results of using the "sharp cutoff" form are similar to using M_2=1.4 GeV. This means that one can obtain the essential features of the realistic matrix elements by choosing appropriate values of M_2.

B. Zero size

We also assume that the hard interaction forms a pointlike configuration. Then,

$$\langle N|\widehat{T}^{\mu}_H(q) = \sum_m \Gamma^{\mu}_{N,m}(q)\langle m| \tag{5.2}$$

$$= C^{\mu}(q)\langle \mathbf{b} = 0|\ , \tag{5.3}$$

where $\Gamma^{\mu}_{N,m}(q)$ is defined in Eq. (4.4). Using the speci-

fied two-dimensional harmonic oscillator model of baryon wave functions, the elastic and inelastic form factors are equal.

Assuming the size of the initial wave packet to be $\mathcal{O}(1/Q)$, instead of zero size, introduces only small numerical corrections to the results shown below. This is because of the effects of wave-packet expansion; the zero-size system expands quickly to a small size $\mathcal{O}(1/Q)$.

VI. NUMERICAL RESULTS

It is simple to obtain explicit evaluations of Eq. (4.16) within the various approximation schemes described in Ref. [16]. The results are lengthy, and can be found in Ref. [33]. Here we display results obtained using the wave function of Eq. (4.16), neglecting the path ordering. The validity of this approximation, called the "exponential approximation" (EA), has been carefully examined and shown to be accurate in Ref. [16] and in Ref. [33].

With explicit expressions for the wave functions in hand, we use Eq. (4.15) and its DWIA limit to calculate the nuclear current matrix element, from which we can construct all of the observables. The kinematics are summarized in Table II. These kinematics are closely related to, but are not exactly those of the experiments [6,7]. This is because our optical potential strengths are only known at energies where previous free NN data have been taken. Predictions for the upcoming experiments can be readily obtained using simple interpolations. For all of our calculations, we take the angle $\beta = \pi/2$ and consider only in-plane scattering. The quantities E_i and θ_e denote the initial electron energy and the electron scattering angle.

A. Integrated differential cross sections

Consider the angular integral, σ, of the $(e, e'p)$ cross section of Eq. (2.3). The ratio $\sigma/\sigma^{\rm Born}$, where the "Born" refers to using a Dirac plane wave for the outgoing proton, is of interest because it is unity in the limit of complete color transparency. These ratios are displayed in Fig. 2 for ^{12}C, ^{40}Ca, and ^{208}Pb. The solid curves (circles) are the DWIA cross sections, divided by the respective

TABLE II. Calculational kinematics.

Q^2 (GeV^2)	E_i (GeV)	θ_e (deg)	$\left(\frac{d\sigma}{d\Omega_{k'}}\right)_{\rm Mott}$ (nb)
0.96	4.0	15.1	1091
1.88	4.0	22.8	203.0
2.38	4.0	27.0	103.6
3.25	4.0	34.8	36.90
4.14	4.0	44.6	13.40
5.96	4.0	84.5	0.8865
5.96	6.0	34.5	17.07
5.96	11.0	22.7	140.7
9.65	15.0	14.7	85.35
20.86	21.0	18.2	18.24

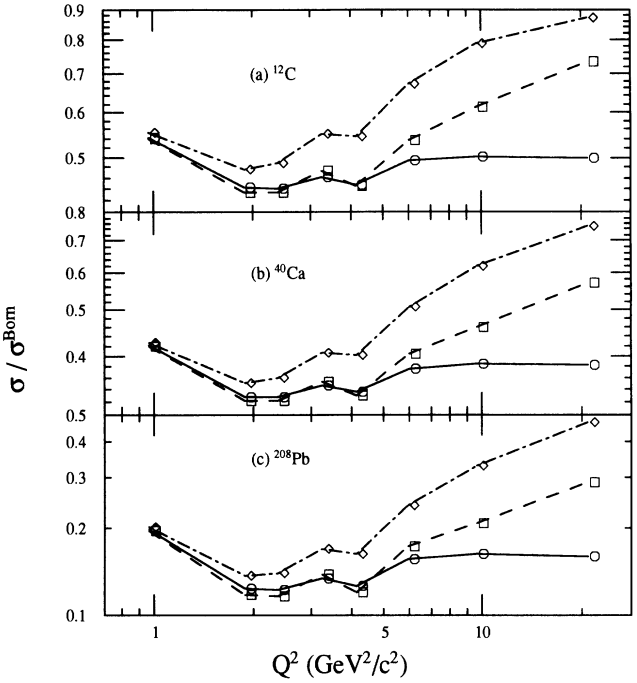

FIG. 2. Total cross section ratios for (a) ^{12}C, (b) ^{40}Ca, and (c) ^{208}Pb. The solid line (circles) is DWIA, the dot-dashed line (diamonds) includes CT, for $M_2 = 1.44$ GeV, dashed lines (boxes) have $M_2 = 1.80$ GeV.

Born cross sections. The dot-dashed curves (diamonds) denote the cross sections, including CT effects, for oscillator spacings of $\Delta M^2 = 1.19$ GeV^2 ($M_2 = 1.44$ GeV). The dashed curves show the cross section ratios, including CT effects, for an excited state mass of $M_2 = 1.80$ GeV. See Table II for the electron kinematics.

There are several noteworthy features about these DWIA and CT results. The first is that the optical potential strengths, obtained from free nucleon-nucleon scattering data, naturally give a DWIA cross section ratio which is large at $Q^2 \approx 1$ GeV^2 and decreases sharply with energy before reaching an asymptotic value. This can be understood by noting that the pp total cross section is only 30 mb at this energy. Thus, we have here an effect similar to the one of Frankfurt, Strikman, and Zhalov [23]. The second dip in the cross section ratios is more difficult to understand but can be traced to the existence of sizable real parts of the Dirac potentials.

Observe also that the DWIA ratios we obtain here are smaller than the results of calculations using scalar photons. For example, for ^{12}C at 20 GeV$^2/c^2$, our DWIA value of $\sigma/\sigma^{\rm Born}$ is 0.50 as compared with 0.54 of Refs. [23,14,36] (using the same pp total cross section of 40 mb). This modest effect is significant for experiments seeking small color transparency effects. The difference between our calculations and the earlier ones is essentially due to the radial dependence of the optical potentials. Ours of Eq. (4.12) have larger values at the origin than those that use the Woods-Saxon shape. The difference may or may not be artificial; the conclusion we draw is that the DWIA result is sensitive (at the 10% level) to details of the nuclear interior which are not yet

determined from other experiments.

Next we discuss the color transparency effects. Recall that NE-18 took measurements at Q^2 =1,3,5 and 6.8 GeV^2. With an excited state mass parameter of 1.44 GeV the cross section at $Q^2 \approx 3$ GeV^2 is the same as at $Q^2 \approx 1$ GeV^2, although at $Q^2 \approx 5$ and 7 GeV^2 the cross section rises rapidly with energy. This equality of the results at $Q^2 \approx 1$ GeV^2 with those of $Q^2 \approx 3$ GeV^2, which simulates the effects of no color transparency, arises from the energy dependence of the nucleon-nucleon scattering data.

The onset of transparency to higher energies can be postponed by simply increasing the value of the first excited state mass, see the dashed curves. The suppression of the transparency for an excited state mass of 1.80 GeV^2 may be too great to agree with the SLAC data at $Q^2 \approx 3$ GeV^2. Thus, it seems that an oscillator spacing such that $M_2 \approx 1.6$ GeV would give a cross section ratio which would appear to be Q^2 independent if one only looked at $Q^2 = 1, 3, 5, 6.8$ GeV^2.

Apart from the energy dependence of the nucleon-nucleon scattering data, the effects of including color transparency are qualitatively similar to the earlier results of Refs. [14,16]. It is natural that the amount of color transparency depends on the precise value of M_2. As noted above, the work of Ref. [34] indicates that values between 1.4 and 1.8 GeV are allowed. A clear indication of color transparency is needed to determine this number. We note that a value of about 1.7 GeV or so allows one to reproduce to BNL (p, pp) data [37].

That the SLAC experiment has seen CT is possible, given the energy dependence of the elementary pp cross section and the optical potential strengths. However, before one can be absolutely sure, it is desirable to take more data points and see what happens at, say, $Q^2 \approx 2$ GeV^2. It would also be nice to increase Q^2 and really see a dramatic rise in the ratio $\sigma/\sigma^{\rm Born}$.

B. Differential cross sections and normal polarizations

The upcoming CEBAF experiment [7] was proposed to test the prediction that the normal polarization should vanish in the limit of complete color transparency. The ^{12}C differential cross sections (as a function of the transverse momentum) and the normal polarizations, to be measured, are displayed in Fig. 3 for low and high values of Q^2. The results for other values of Q^2 and for ^{40}Ca and ^{208}Pb are presented in Ref. [33]. The figures are labeled by E_i, the initial energy of the incident electron. Different values of E_i affect only the electron kinematics that are part of $|\mathcal{M}_{\alpha,\check{s}_R}|^2$. These are the first detailed predictions of these angular observables which include the effects of CT.

Figure 3 clearly displays the shell structure of the ^{12}C nucleus. For instance, ^{12}C has four p-shell protons and only two s-shell ones. The wave functions for the s-shell nucleons peak at the origin, of course, while the p-shell ones have a node there. This is why the cross section for ^{12}C has a maximum at about $q_\perp \approx 0.5$ fm^{-1}. Similarly, the shell structure for ^{40}Ca and ^{208}Pb can be discerned from the figures in Ref. [33].

Our predictions are that the energies proposed in the experiments are *not* high enough to see the normal polarization vanish. CT effects strong enough to enhance the total cross section by 40% (high mass case) do not lead to a strong suppression of the normal polarization. However, in ^{12}C there is a measurable suppression of the polarization for the CT-included case of light excited state mass ($M_2 = 1.44$ GeV). A detailed comparison with the SLAC NE-18 results would be necessary to see if using the light excited state mass is still viable. In ^{40}Ca and ^{208}Pb there is only a small suppression of the normal polarization even at $Q^2 = 20$ GeV^2.

Thus, it seems that the normal polarization is a diffi-

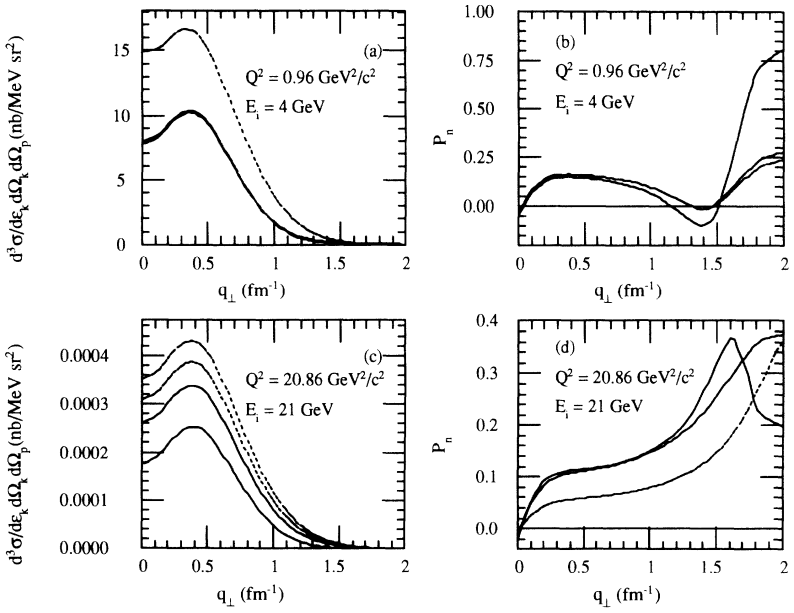

FIG. 3. Differential unpolarized cross section and normal polarization for ^{12}C at $Q^2 = 0.96$ GeV^2 and at $Q^2 = 20.86$ GeV^2. The curves are as in Fig. 2.

cult quantity in which to observe CT effects. However, a precise experiment could be successful.

C. The normal-transverse response of ^{208}Pb

The total differential cross sections and normal polarizations are constructed from kinematically weighted sums of bilinear combinations of the components of $\mathcal{J}^{\mu}_{\alpha,\check{\mathbf{s}}}\mathcal{J}^{\nu *}_{\alpha,\check{\mathbf{s}}}$, where $\check{\mathbf{s}}$ is some spin direction. These components are sometimes called "response functions" [24]. We have shown how to calculate a CT-included wave function which allows a construction of the nuclear current matrix element. Once done, it is simple to explicitly construct all of these individual components or response functions. Since these quantities are more difficult to measure than total angular distributions, and Saha is not planning on doing so, we omit most of these results. However, these response functions, for a number of values of Q^2 and for our three nuclei (^{12}C, ^{40}Ca, ^{208}Pb), have been computed [33] and are available on request.

We do show one striking feature which has emerged from our systematic study of the response functions. In lead, there is strong absorption and the effects of CT do not manifest themselves until very high energies, making the experimental verification of CT in lead unlikely if one looks only at unpolarized observables. However, in one of the spin-dependent responses, we see something quite different and quite interesting. In Fig. 4 we display the quantity R^n_T as a function of $q_\perp$. R^n_T is called the "normal-transverse response" since it depends on spin asymmetries normal to the photonuclear scattering plane (along the X axis here) of bilinear products of the transverse components of the current; see Eq. (2.4) and the discussion below. Looking at Fig. 4, we see that for both light and heavy excited state mass cases there is a huge enhancement in the region of $q_\perp \approx 0.4$–1.5 fm^{-1}. That is, a ratio of CT response to DWIA response ranges all the way from zero to infinity over this angular range.

We note that R^n_T vanishes when the plane-wave approximation is valid, so that one may wonder if this "large" value of R^n_T is a CT effect at all. A close examination, which we now explain, shows that it is. Obtaining a nonzero value of R^n_T depends on having an interference between a central and spin-orbit interaction. The spin-orbit interaction can occur in the bound state or the ejectile state. The bound-state spin-orbit force is particularly large in the $1H_{11/2}$ orbital. For this orbital, the interference between a strong bound-state spin-orbit effect and a reduced central final-state interaction produces the computed CT results. With the effects of CT reducing both central and spin-orbit interactions in the scattering state, the other orbitals produce very little effect in R^n_T. This is because the bound-state spin-orbit forces are smaller for other orbitals and the contributions from orbits with $j = l + 1/2$ tend to cancel those from orbits of $j = l - 1/2$. Thus, when CT is included, it is the $1H_{11/2}$ orbital that is almost entirely responsible for the value of R^n_T in the region of $q_\perp \approx 0.4 - 1.5$ fm^{-1}. For the DWIA, there is no suppression of central and spin-orbit forces in the scattering state. In DWIA, the contribution to R^n_T from the $1H_{11/2}$ orbital is very similar to that obtained including CT effects. The reason is that this orbital is at the edge of the nucleus where distortion effects are reduced. However, for the DWIA calculation, the other orbitals, taken together, contribute equally in magnitude (to the $1H_{11/2}$) but opposite in sign. This is because the spin-orbit force is repulsive for the scattering wave, but is attractive for the bound state. Also, the sum of contributions from states with $j = l \pm 1/2$ is negative in this angular range, due to the differences in the radial parts of the bound-state wave functions. The net result is the nearly complete cancellation observed in Fig. 4. A cancellation of this type occurs in all DWIA models.

Thus a detected value of R^n_T of the size shown, could be an unambiguous signature of CT. This enhancement begins at momentum transfers as low as $Q^2 \approx 2$ GeV^2 and continues to the highest energies. However, the separation of this response function from the total normal polarization may be difficult. In fact, our predictions for R^n_T and for the other response functions [33] indicate that the transverse-normal response only contributes about one part in 20 to the polarization. The predictions presented here, however, indicate that attempting this separation may be worthwhile.

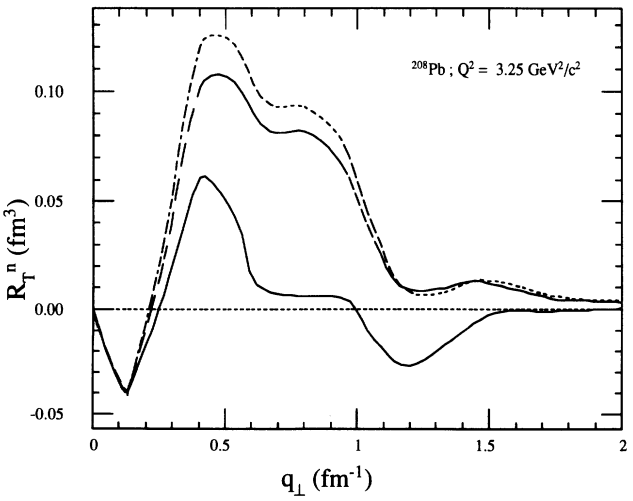

FIG. 4. Normal-transverse response function for ^{208}Pb at $Q^2 = 3.25$ GeV^2. The curves are as in Fig. 2.

D. Gauge invariance and current conservation

Computations of the nuclear current matrix element (NCME) should be consistent with the requirements of of gauge invariance and current conservation (CC). Previous calculations of CT effects in $(e, e'p)$ reactions seem to use a scalar photon; no information about the individual components of the current four-vector appears. The present relativistic calculation gives us an opportunity to study these components and see if CC holds.

It is well known that DWIA calculations of this type may suffer from a lack of CC. This is due to the truncation of a problem involving many nucleons into a one-nucleon problem. Indeed, CC can be recovered by gen-

eralizing the electromagnetic current operator to include the effects of states with two particles in the continuum. But at high energies, such effects are small and the error made by ignoring such many-body effects is much smaller than the errors obtained by artificially imposing CC [38,39].

This problem could also afflict our work. We do not wish to impose CC in an artificial manner, but we must check that the current is at least approximately conserved. There are many ways that one can consider quantifying current conservation violation (CCV). We would like to investigate how the CCV's change as a function of Q^2, so, we define the angle-integrated quantity

$$\mathcal{W}^{\mu\nu} \equiv \frac{2\pi}{|\mathbf{q}|^2} \sum_{\alpha,\check{\mathbf{s}}_R} \int dq_\perp \, q_\perp \, \mathcal{J}^{\mu *}_{\alpha,\check{\mathbf{s}}_R}(q) \mathcal{J}^{\nu}_{\alpha,\check{\mathbf{s}}_R}(q) \ , \quad (6.1)$$

where $\mathcal{J}^{\nu}_{\alpha,\check{\mathbf{s}}_R}$ is defined in Eq. (4.2), the sum on α is over all occupied shells, and the sum on $\check{\mathbf{s}}_R$ is over both rest-frame spin projections. The quantity $q_\perp = |\mathbf{p} - \mathbf{q}| \approx |\mathbf{q}| \sin\zeta$, where ζ is the angle between the virtual photon and the ejected proton. Choosing the $\check{\mathbf{Z}}$ direction to be defined in the direction of $\mathbf{q}$, gauge invariance requires

$$\Delta R_L \equiv \frac{q_0^2 \mathcal{W}^{00} - q_3^2 \mathcal{W}^{33}}{q_0^2 \mathcal{W}^{00} + q_3^2 \mathcal{W}^{33}} \quad (6.2)$$

to be zero. We display results for ΔR_L as a function of Q^2 for ^{12}C, ^{40}Ca, and ^{208}Pb, and for both internal oscillator spacings, $M_2 = 1.44$ GeV (light) and $M_2 = 1.80$ GeV (heavy).

Figure 5 shows that our calculation violates current conservation at the 10% level for the DWIA at the lowest energies but only at the 3–4 % level for the CT cases. The CCV decreases as the value of Q^2 increases. Notice that the current is mostly conserved for the plane-wave cases, becoming less so for the heavier nuclei.

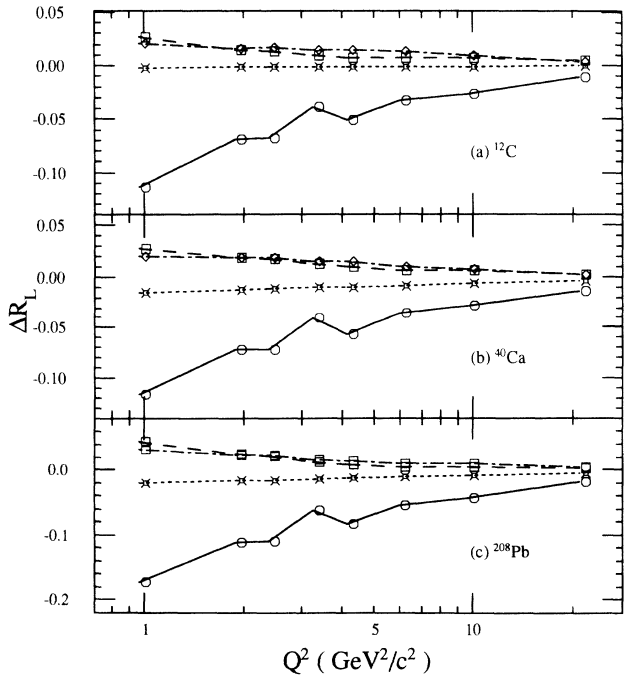

FIG. 5. Current conservation violations for (a) ^{12}C, (b) ^{40}Ca, and (c) ^{208}Pb. The solid, dot-dashed, and dashed curves are as in Fig. 2; the new dotted curve is the Born approximation.

In our view, even the largest CCV of 10% is not a very serious problem. Such an uncertainty is comparable to the uncertainties caused by a lack of detailed knowledge about the radial shape of the optical potential, as well as the lack of sufficiently precise nucleon-nucleon phase shifts. Furthermore, the 10% violation of CC corresponds to a smaller uncertainty in the cross sections and normal polarizations because of their dependence on the transverse components of the current which are not constrained by CC. Thus we conclude that our calculation satisfies CC to a sufficiently high accuracy.

Of course, in nature, current is conserved exactly. However, we make the provocative statement that the improvement of current conservation in our calculation over the traditional Glauber treatment (when the CT effects do not strongly enhance the cross section) provides some evidence that CT effects are necessary for an accurate theoretical treatment of $(e, e'p)$ reactions.

E. Fermi motion

It has recently been argued [23,37,40,41] that the Fermi motion of the nucleons bound in the nucleus strongly enhances the effects of color transparency. Suppose, in the $(e, e'p)$ reaction, that the virtual photon three-momentum is labeled by $\mathbf{q}$ and the detected proton three-momentum is called $\mathbf{p}$. Let $\mathbf{p} = \mathbf{q} + \mathbf{k}$. Sometimes $\mathbf{k}$ is called the "momentum of the struck nucleon," which it is in the Born approximation (the CT limit). But final-state interactions can influence the outgoing proton's longitudinal momentum. In exactly quasielastic kinematics, the bound nucleon is treated as at rest and free and so $\mathbf{k} = 0$. Fermi motion causes nonzero values. In the above calculations, we have assumed that $\mathbf{k} = \mathbf{q}_\perp$ where $\mathbf{q}_\perp$ is very small in magnitude, $|\mathbf{p}| \approx |\mathbf{q}|$, and is purely transverse to $\mathbf{q}$. This assumption leads to the differential distributions in Sec. VI and in Ref. [33].

It has been shown [37,40,41] that the component of $\mathbf{k}$ which is parallel (or antiparallel) to $\mathbf{q}$ has a huge numerical effect on the calculated transparencies. This is investigated here. Let the component of $\mathbf{k}$ in the $\check{\mathbf{q}}$ direction be called $k_\parallel$. Thus, $\mathbf{k} = k_\parallel \check{\mathbf{Z}} + \mathbf{q}_\perp$. Nonzero values of $k_\parallel$ are especially important in (p, pp) reactions [23] because the experimental results of Refs. [3,4] are presented in terms of bins of $k_\parallel$.

We have calculated the cross sections and other observables for $Q^2 = 0.96$ and 20.86 GeV^2 for values of $k_\parallel = -150, -75, 0, 75$, and 150 MeV. In particular, we assume that $\mathbf{p} \cdot \check{\mathbf{Z}} = |\mathbf{q}| + k_\parallel$, where $\mathbf{q}$ is in the Z direction. The results for the total cross section ratios and the CCV measure ΔR_L are shown in Fig. 6.

In all of the figures we display four curves. The dotted curve is the Born approximation, the solid curve is the DWIA, and the dot-dashed and the dashed lines are CT results for light and heavy excited state masses. In the plots for the cross section ratios, we display the ratios for

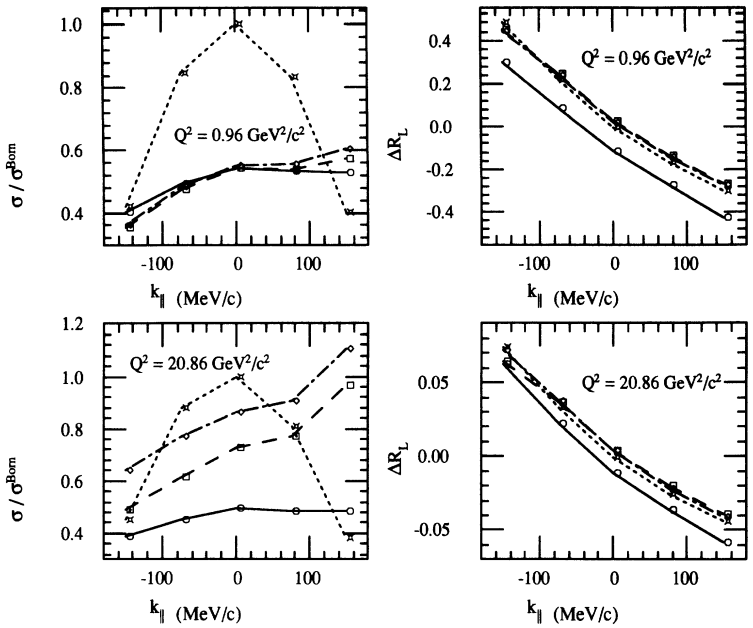

FIG. 6. Effect of Fermi motion.

the cross section at $k_{||}$ divided by the Born cross section at that same value of $k_{||}$, except for the Born curve, which is the cross section at $k_{||}$ divided by the Born cross section at $k_{||} = 0$. At low energies, the effect of finite $k_{||}$ is pretty small on the cross section ratios, about 20%. At high energies, the effect is quite large for the CT cases, although still a small effect for the DWIA. However, nonzero values for $k_{||}$ lead to a large reduction, over a factor of 2, in the Born cross section at low and high energies.

Another result from these calculations is shown in the measure of CCV. In particular, we see that as $k_{||}$ moves away from zero, current conservation is violated more and more, reaching the 40% level for $|k_{||}| = 150$ MeV/c, at $Q^2 = 0.96$ GeV^2. At higher Q^2, the situation improves so that the violations are at the 5% level. Clearly, violations of 40% or more are intolerable and our calculation probably cannot be trusted there. We display these results only because we expect this problem to occur also in the scalar photon work of [40,41] who have advocated measurements at $|k_{||}| = 150$ MeV/c to enhance the effects of color transparency.

Violations of 5% probably do not affect the physics too much. Thus, there is no problem in trusting our calculation at high Q^2 or at small values of $k_{||}$.

The most important cause of CCV in our calculation is probably coming from the lack of orthogonality between the initial-state and final-state wave functions, caused by the truncation of a many-body problem to a one-body problem. Indeed, we have left out effects in the initial state, such as particle-hole excitations as well as explicit isobar degrees of freedom which can alter the nucleon-nucleon force. Also, we have ignored the possibilities that the nucleons are altered in the medium and that the current operator might not be a free-nucleon operator. Another possibility is to express the observables in terms of the "good" components of the current as advocated by Frankfurt and Strikman [42]. A more careful treatment of some of these effects could lead to improvements in the gauge invariance of our models.

F. Lower components

We examine the effects of the lower components by artificially setting these to zero in the scattered wave function. The results for the integrated cross section ratios are shown in Fig. 7(a). The solid and dot-dashed curves are calculated using the DWIA and CT wave functions with the lower components turned off, divided by the Born calculation also with no lower components. The dotted curve in Fig. 7 is the ratio of the Born calculation with no lower components to the Born calculation with lower components. The figure shows a striking effect: the lower components are not significant in the predicted cross section ratios. This is actually quite amazing since the Born calculation changes so much when the lower components are turned off.

However, we point out that these lower components are crucial to the approximate satisfaction of current conservation, see Fig. 7(b). We conclude that the lower components are essential to our description of the ejectile wave function. Without these inherently relativistic components we would lose approximate current conservation, although the integrated cross section ratios remain unchanged. A more complete discussion of the role of the lower components in both the scattered and bound states is described in Ref. [33].

VII. SUMMARY AND CONCLUSIONS

This paper is concerned with explicitly including the effects of proton and photon spin in quasielastic $(e, e'p)$ and $(e, e'\vec{p})$ reactions at large momentum transfers. If CT occurs, a rapidly moving small-sized wave packet is formed when the photon is absorbed by a bound proton. The main motivation for including the effects of spin is the proposal by Saha and collaborators [7] who plan to measure the normal component of the proton polariza-

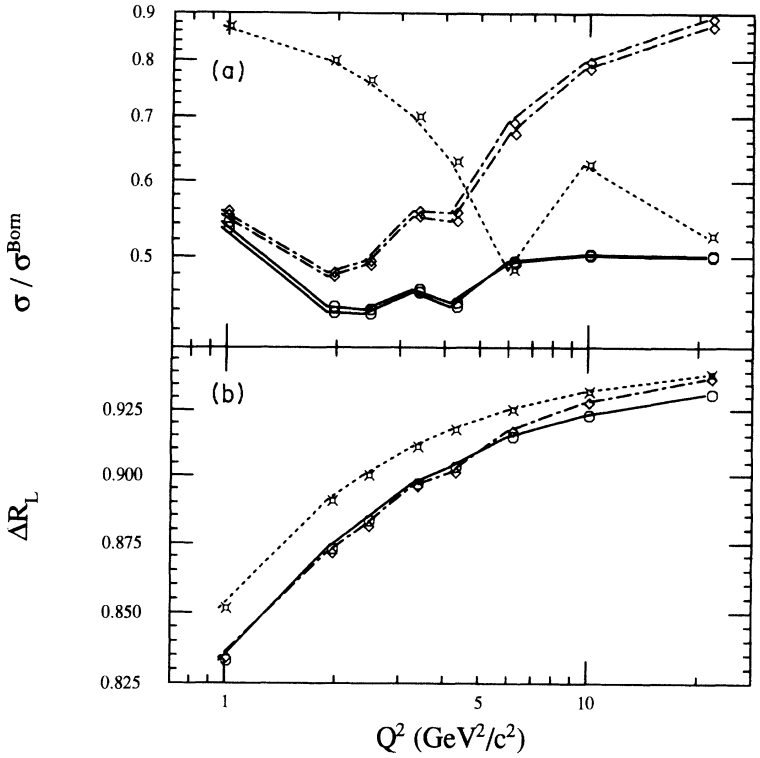

FIG. 7. (a) Total cross section ratio for ^{12}C using wave functions with no lower components. The ratio is independent of the lower components. (b) Current conservation violations for ^{12}C using wave functions with no lower components.

tion P_n in $(e, e'\vec{p})$ experiments. The vanishing of P_n is a signature of color transparency. Further, the photon really is a vector particle and its spin should play some role in the scattering. Dirac phenomenology is used to construct the DWIA and, the effects of CT are included by treating the ejected wave packet as a linear superposition of four-component states. The principal formal result is the wave function of Eq. (4.16).

CT effects are expected to be present in other reactions such as (p, pp), $(\pi, \pi p)$, etc. The wave function in Eq. (4.16) can also be used to study those reactions.

In our approach to CT, it is necessary to choose an explicit form for the wave-packet–nucleon interaction. We choose Eq. (5.1) which is consistent with the known constraints. It is also necessary to assume a model for the baryon spectrum. We use that of a two-dimensional transverse harmonic oscillator. With this choice comes a single free parameter, the oscillator spacing, which determines the masses of the nucleon resonances. This spacing is characterized by the mass of the first even parity excited state, labeled by M_{N^*} or M_2. Here we use the values $M_2 = 1.44$ GeV and $M_2 = 1.80$ GeV, which the reader may use to reconstruct the more realistic spectrum of Ref. [34].

Although we use simplified models for the wave-packet–nucleon interaction and the internal baryon space, the methods of calculation presented in this paper are more general and can be used with more realistic interactions and models.

We calculate ratio of cross sections for ^{12}C, ^{40}Ca, and ^{208}Pb as a function of Q^2. We use the cross section and other optical potential strengths derived directly from data taken at different energies. The result is that we confirm the assertion of Frankfurt, Strikman, and Zhalov, that energy dependence in $\sigma/\sigma^{\rm Born}$ is expected. This is because the pp cross section, in the energies of the experiment [6], varies in such a way that the Glauber treatment decreases the transparency ratio. Therefore, since the preliminary results of the experiment see a small variation in the ratio as a function of Q^2, CT effects may be offsetting the Q^2 variation predicted by the DWIA. Furthermore, we find that the Dirac DWIA calculations lead to predictions of σ/σ^B some 10% smaller than earlier DWIA calculations. This is because the shell model leads to slightly larger optical potentials near the center of the nucleus, where they are not well constrained by data.

We also compute the spin observables. We display results for differential cross sections and normal polarizations. The differential cross sections display a noticeable, and detectable, increase at large momentum transfers. This is responsible for the CT effects in the integrated cross section ratios described above. However, our calculations of P_n show no significant deviations from the usual Glauber treatment. A possible exception is for $Q^2 \approx 20$ GeV^2 where in ^{12}C a moderate decrease of the polarization is obtained for case of $M_2 = 1.44$ GeV but not for $M_2 = 1.8$ GeV. We conclude that the energies at which the normal polarization should completely vanish are, unfortunately, quite high, in the vicinity of Q^2=100 GeV^2. Frankfurt, Strikman, and Zhalov have obtained a similar result [43].

We also calculate the individual separated response functions. In particular, we find that CT effects lead to a strong enhancement of the computed value of the normal-transverse response R_T^n for $|\mathbf{q}_\perp| \approx 0.5 - 1$ fm^{-1} with $Q^2 \geq 2$ GeV^2. That this is due to the strong effects of the $1H_{11/2}$ orbital is explained in Sec. VI.

A typical possible problem with calculations of this

sort is the lack of current conservation CC. We show that the violations of CC are at the 10% level for the DWIA and only at the 4% level for the CT wave functions at low energies, but are all at the 1–2 % level at the highest energies, $Q^2 \approx 20$ GeV^2. Inclusion of CT effects is therefore desirable, even at low energies, because it improves the consistency with the requirements of CC. We also argue that a 10% violation of CC corresponds to a smaller uncertainty in the observables which depend also on transverse components of the current which are not constrained by CC. Thus CC is conserved to a sufficiently high accuracy.

We also study the effects of Fermi motion of the initial nucleon, which can have a big effect on the cross section ratios if the "initial nucleon momentum" is along the direction of $\mathbf{q}$ [40,41]. Indeed, for values of $k_{\|} \gtrsim 150$ MeV/c, which is this component, the violations of current conservation become severe at low energies and our calculation and probably others [40,41] cannot be trusted there. At high energies, the violations of CC become smaller and we find that the ratio $\sigma/\sigma^{\rm Born}$ increases rapidly as $k_{\|}$ increases.

The effects of the lower components on cross section ratios, current conservation, polarization, etc., are also examined. We find that the total cross section ratios are completely insensitive to the lower components of the scattered wave functions. However, the lower components are crucial, in our model, for the approximate conservation of current.

In conclusion, we make the following short comments. The recent SLAC data [6] imposes constraints on the allowable models shown in this paper. Despite the lack of significant Q^2 variation in the data it is possible, because of the energy dependence of the elementary pp observables, and because our DWIA results for the cross section ratios are smaller than earlier calculations, that the data may be an example of the manifestation of CT. A measurement of the normal polarization in $(e, e'\vec{p})$ reactions does not seem to be a good way to see CT effects at moderate Q^2. However, a measurement of the normal transverse response in a heavy nucleus such as ^{208}Pb does seem to afford the opportunity to see CT, unambiguously, at quite low momentum transfers.

ACKNOWLEDGMENTS

We wish to thank B. Jennings, L. Frankfurt, and M. Strikman for useful discussions, and C. Horowitz for his computer code. This work was supported in part by the U.S. Department of Energy.

APPENDIX: OPTICAL POTENTIAL STRENGTHS

We describe how the strengths of the scalar and vector optical potentials of Eq. (3.3) and Table I are obtained from proton-proton elastic scattering data.

1. Optical potential

Start with a standard parametrization of the nucleon-nucleon scattering amplitude given by

$$\frac{f_c}{2ik} = A + B\boldsymbol{\sigma}_1 \cdot \boldsymbol{\sigma}_2 + iqC\,(\sigma_{1n} + \sigma_{2n}) + D\boldsymbol{\sigma}_1 \cdot \mathbf{q}\,\boldsymbol{\sigma}_2 \cdot \mathbf{q} + E\sigma_{1Z}\sigma_{2Z}, \quad \text{(A1)}$$

where k is the center-of-mass momentum and $\sigma_a = \boldsymbol{\sigma} \cdot \boldsymbol{a}$. One can also parametrize the NN scattering amplitude in a Lorentz invariant form in terms of Dirac matrices,

$$F = F_s + F_v\gamma_1^\mu\gamma_{2\mu} + F_t\sigma_1^{\mu\nu}\sigma_{2\mu\nu} + F_p\gamma_1^5\gamma_2^5 + F_a\gamma_1^5\gamma_2^5\gamma_1^\mu\gamma_{2\mu}. \quad \text{(A2)}$$

We are concerned with the case of elastic scattering of protons from nuclei. In the relativistic impulse approximation, the T matrix for nucleon-nucleus scattering is a sum of bound nucleon matrix elements of free nucleon-nucleon t matrices proportional to F. In a spin saturated nucleus, only the scalar, vector, and tensor terms are nonvanishing. The coordinate space optical potential is obtained by Fourier transforming the momentum space potential. In the limit of very high energies, the scattering is predominantly in the forward direction. Thus, we can approximate $F_s(q)$ and $F_v(q)$ by their forward direction values F_s^0 and F_v^0, and neglect the tensor term. Thus, we arrive at [18]

$$U_{\rm opt}(\mathbf{R}) = -\frac{4\pi i p_{\rm lab}}{M_N}\left[F_s^0\rho_s(R) + \gamma_1^0 F_v^0\rho_v(R)\right], \quad \text{(A3)}$$

where $p_{\rm lab}$ is the laboratory-frame momentum and the superscript 0 here and below denotes that the forward scattering amplitude is used.

In the forward scattering approximation, the relationship between the Pauli and Dirac amplitudes can be written as a matrix equation [27]. Since A, B, C, D, E are to be taken from data, we invert this matrix to obtain the scalar and vector density strengths from the Pauli amplitudes. In particular,

$$F_s^0 = \frac{1}{2\xi^2(1+\xi)}\left[\xi(2\xi+1)A^0 + (2\xi^2-1)B^0 + 2M_N\xi(2\xi^2-1)\sqrt{\frac{\xi+1}{\xi-1}}C^0 + \frac{1-2\xi^2}{2(\xi-1)}E^0\right], \quad \text{(A4)}$$

$$F_v^0 = \frac{1}{2\xi^2(1+\xi)}\left[\xi A^0 - B^0 - 2M_N\xi\sqrt{\frac{\xi+1}{\xi-1}}C^0 + \frac{1}{2(\xi-1)}E^0\right], \quad \text{(A5)}$$

where $\xi = \sqrt{s}/2M_N$ and the quantity D^0 no longer appears.

2. Extracting forward amplitudes from data

We extract the NN parameters A^0, B^0, C^0, E^0 from the data using two methods. In the first, recent phase

shift solutions are used. The second involves a more direct determination of the relevant amplitudes from data.

a. Forward amplitudes from $Q^2 = 1 - 6$ GeV^2

Wallace has published [28] the Pauli amplitudes, A^0, B^0, C^0, D^0, E^0 for Hoshizaki's phase shift solutions up to $Q^2 = 4$ GeV^2 [29]. Therefore, we construct the optical potential strengths in this energy regime by using Eqs. (A4) and (A5) for Wallace's amplitudes.

At higher energies, we use the phase shift analysis of Higuchi and Hoshizaki [30] for pp phase shifts at $p_{\rm lab} = 4$ GeV, which translates to $Q^2 = 5.96$ GeV^2, in order to reconstruct the T matrix and extract the strengths as outlined.

The phase shifts are only loosely constrained at these energies and, different phase shift analyses yield different values for the optical potential strengths. However, our strengths are roughly consistent with those found in Ref. [27].

b. Forward amplitudes at $Q^2 = 9.65$ and 20.86 GeV^2

At higher energies, more and more partial waves are required (and the data become more and more scarce) so phase shift analyses become difficult. However, phase shift analyses do exist [31] for (laboratory) beam momenta of 6 GeV/c and 12 GeV/c; in quasielastic kinematics, these beam momenta translate to $Q^2 = 9.65$ and 20.86 GeV^2. However, the lack of constraining data and the problem that the high angular momentum partial waves are not negligible and must be modeled leads us away from using phase shifts. However, we do take certain qualitative features from these analyses; see below. Further, the phase shift analyses do not emphasize the forward direction observables over the other angles. Indeed,

$$A^0 = \frac{\sigma}{8\pi}\left(1 - i\alpha_f\right), \tag{A6}$$

$$B^0 = \frac{\Delta\sigma_T}{-16\pi} - i\frac{F_2}{4k}, \tag{A7}$$

$$E^0 = \frac{\Delta\sigma_L}{-16\pi} + i\frac{F_3}{4k} - B^0, \tag{A8}$$

where α_f is the ratio of the real part to the imaginary part of the forward scattering amplitude and k is the center-of-mass momentum. The other imaginary parts F_2 and F_3 are evaluated using dispersion relations [44].

Thus, the only required quantity not available directly from the forward cross section data is the parameter C^0. However, this parameter can be obtained if enough data on the spin observables at small $-t$ are known. For instance, in the four-index notation of Ref. [45], we can write two of the spin observables as

$$\frac{d\sigma}{dt} P_{n000} = 8\pi q \,\mathrm{Im}\,(A + B)\, C^*, \tag{A9}$$

$$\frac{d\sigma}{dt} A_{00sk} = -\frac{4\pi q}{k}\mathrm{Re}\left\{\left[(A^* + B^*)\sqrt{1 - \frac{q^2}{4k^2}} + 2k\left(1 - \frac{q^2}{2k^2}\right)C^*\right]\left[q^2 D - E\right]\right\}. \tag{A10}$$

Notice that both P_{n000} and A_{00sk} vanish in the forward direction ($q = 0$). Their slopes (as a function of q, not $-t$) at $q = 0$, however, are finite. Taking the derivatives of Eqs. (A9) and (A10) with respect to $q = |\mathbf{q}| = \sqrt{-t}$ and evaluating in the forward direction, it is possible to solve for the real and imaginary parts of C in terms of the spin data:

$$C_R^0 = \frac{\left(\frac{d\sigma}{dt}\right)_{t=0}\left[E_I^0\left(\frac{dP_{n000}}{dq}\right)_{q=0} + \left(\frac{dA_{00sk}}{dq}\right)_{q=0}\right]}{8\pi\,\mathrm{Re}\,(A^0 + B^0)\,\mathrm{Re}\,[(A^0 + B^0)\,E^{0*}]} - \frac{1}{2k\mathrm{Re}\,(A^0 + B^0)}, \tag{A11}$$

$$C_I^0 = -\frac{A_I^0 + B_I^0}{A_R^0 + B_R^0} C_R^0 - \frac{1}{8\pi}\left(\frac{d\sigma}{dt}\right)_{t=0}\left(\frac{dP_{n000}}{dq}\right)_{q=0}, \tag{A12}$$

where x_R^0 and x_I^0 denote the real and imaginary parts of the complex number x, evaluated in the forward direction. Thus, with these equations, and some good spin data, we can extract the optical potential strengths directly from data.

The experimental values for the $\sigma^{\rm tot}$, α_f, $\Delta\sigma_L$, $\Delta\sigma_T$, F_2, and F_3 are summarized in Ref. [31]. In order to complete the analysis described above, we need information on the slopes of P_{n000} and A_{00sk} at small q. In Refs. [46] the polarization P_{n000} has been measured at $p_{\rm lab} = 6$ GeV/c. Better than that, an empirical fit to the data is given, which can be directly differentiated. By averaging these two values from the two references, we obtain the result

$$\left(\frac{dP_{n000}}{dq}\right)_{q=0} = 0.494 \text{ GeV}^{-1} \quad \text{for } p_{\rm lab} = 6\,\text{GeV}/c. \tag{A13}$$

TABLE III. Forward scattering data at $p_{\rm lab} = 6$ and 12 GeV/c.

$p_{\rm lab} = 6$ GeV/c					
$\sigma^{\rm tot}$	=	40.75 mb	α_f	=	−0.32
$\Delta\sigma_T$	=	0.35 mb	F_2	=	−4.60 GeV^{-1}
$\Delta\sigma_L$	=	−1.04 mb	F_3	=	4.60 GeV^{-1}
$\left(\frac{d\sigma}{dt}\right)_{t=0}$	=	93.0 mb	$\left(\frac{dP_{n000}}{dq}\right)_{q=0}$	=	0.494 GeV^{-1}
$p_{\rm lab} = 12$ GeV/c					
$\sigma^{\rm tot}$	=	39.60 mb	α_f	=	−0.29
$\Delta\sigma_T$	=	0.01 mb	F_2	=	−6.05 GeV^{-1}
$\Delta\sigma_L$	=	−0.73 mb	F_3	=	3.55 GeV^{-1}
$\left(\frac{d\sigma}{dt}\right)_{t=0}$	=	65.0 mb	$\left(\frac{dP_{n000}}{dq}\right)_{q=0}$	=	0.215 GeV^{-1}

TABLE IV. Pauli amplitudes for pp scattering.

Q^2 (GeV^2)	A^0 (GeV^{-2})	B^0 (GeV^{-2})	C^0 (GeV^{-3})	E^0 (GeV^{-2})
0.96	$3.08 - 1.31i$	$-0.22 + 1.21i$	$-1.76 - 6.55i$	$0.69 + 0.02i$
1.88	$4.87 + 0.81i$	$-0.23 + 1.03i$	$-3.13 - 5.44i$	$0.82 - 0.05i$
2.38	$4.85 + 1.06i$	$-0.38 + 0.71i$	$-3.11 - 5.22i$	$0.81 + 0.16i$
3.25	$4.70 + 1.86i$	$-0.14 + 0.48i$	$-2.81 - 3.35i$	$0.29 + 0.16i$
4.14	$4.53 + 1.34i$	$-0.05 + 0.47i$	$-3.41 - 3.95i$	$0.15 - 0.01i$
5.96	$4.31 + 1.13i$	$-0.04 + 0.40i$	$-1.62 - 2.13i$	$0.12 - 0.09i$
9.65	$4.16 + 1.33i$	$-0.02 + 0.19i$	$-1.34 - 1.62i$	$0.07 - 0.00i$
20.86	$4.05 + 1.17i$	$-0.00 + 0.13i$	$-1.61 - 0.87i$	$0.04 - 0.05i$

The uncertainty in this quantity is only about 3%; see Ref. [46]. At $p_{\rm lab} = 12$ GeV/c, the polarization has been measured [47] and again an empirical fit is given. Thus, differentiating this quantity directly we find that

$$\left(\frac{dP_{n000}}{dq}\right)_{q=0} = 0.215\,\text{GeV}^{-1} \quad \text{for } p_{\rm lab} = 12\,\text{GeV}/c. \tag{A14}$$

To proceed, we now notice that the data for A_{00sk} at $p_{\rm lab} = 4$ GeV/c [30] shows that the slope of A_{00sk} (with q) is approximately zero. Indeed, explicit calculation based on Hoshizaki's phase shifts yield a slope of 0.014 GeV^{-1}, at $Q^2 = 4.14$ GeV^2. There are very little data for A_{00sk} at higher energies, yet the phase shift solutions [31] also suggest that the slope of A_{00sk} is very small. Based on this evidence, we assume that

$$\left(\frac{dA_{00sk}}{dq}\right)_{q=0} = 0, \tag{A15}$$

at least for energies below $p_{\rm lab} = 12$ GeV/c.

Using the central values in the published data yields optical potential strengths which are larger in magnitude than the lower-energy values. However, by adjusting the parameters within their experimental error bars, numbers in better agreement (more consistent) with the low-energy data can be obtained. It is these numbers which are summarized in Table I. There is therefore considerable uncertainty in the last two rows of Table I. In particular, the forward scattering data we use to generate the strengths are displayed in Table III.

The Pauli amplitudes (A^0, B^0, etc.) are displayed in Table IV. The most important of these parameters are A^0, which contains the information about the forward scattering amplitude, and the spin-flip parameter C^0 which is determined from the slopes of the forward spin observables.

[1] A. H. Mueller, in *Proceedings of the Seventeenth Rencontre de Moriond*, Moriond, 1982, edited by J. Tran Thanh Van (Editions Frontieres, Gif-sur-Yvette, France, 1982), p. 13.

[2] S. J. Brodsky, in *Proceedings of the Thirteenth International Symposium on Multiparticle Dynamics*, edited by W. Kittel, W. Metzger, and A. Stergiou (World Scientific, Singapore, 1983).

[3] A. S. Carroll *et al.*, Phys. Rev. Lett. **61**, 1698 (1988).

[4] S. Heppelmann, in *Nuclear Physics on the Light Cone*, edited by M. B. Johnson and L. S. Kisslinger (World Scientific, Singapore, 1989), p. 199.

[5] A. S. Carroll *et al.*, BNL Experiment 850.

[6] R. McKeown and R. Milner, spokesmen, NE-18 (SLAC) collaboration, at the 1992 Meeting of the Division of Nuclear Physics of the American Physical Society in Santa Fe, NM, October, 1992; N. C. R. Makins *et al.*, Phys. Rev. Lett. **72**, 1986 (1994).

[7] A. Saha *et al.*, "Study of Nuclear Medium Effects by Recoil Polarization up to High Momentum Transfers," CEBAF proposal PR91-006. Proposed and approved.

[8] F. E. Low, Phys. Rev. D **12**, 163 (1975); S. Nussinov, Phys. Rev. Lett. **34**, 1286 (1975); J. Gunion and D. Soper, Phys. Rev. D **15**, 2617 (1977); B. Povh and J. Hufner, Phys. Rev. Lett. **58**, 1612 (1987); G. Bertsch *et al.*, *ibid.* **47**, 297 (1981).

[9] L. Frankfurt and M. Strikman, Phys. Rep. **160**, 235 (1988), Prog. Part. Nucl. Phys. **27**, 135 (1991); B. Z. Kopeliovich, Fiz. Elem. Chastits At. Yadra **21**, 419 (1990) [Sov. J. Part. Nucl. Sci. **21**, 177 (1990)].

[10] L. Frankfurt, G. A. Miller, and M. Strikman, Comments Nucl. Part. Phys. **21**, 1 (1992).

[11] H-n Li and G. Sterman, Nucl. Phys. **B381**, 129 (1992).

[12] L. Frankfurt, G. A. Miller, and M. Strikman, Nucl. Phys. **A555**, 752 (1993).

[13] G. R. Farrar, H. Liu, L. L. Frankfurt, and M. I. Strikman, Phys. Rev. Lett. **61**, 686 (1988); B. Z. Kopeliovich and B. G. Zakharov, Phys. Lett. B **264**, 434 (1991); Phys. Rev. D **44**, 3466 (1991).

[14] B. K. Jennings and G. A. Miller, Phys. Rev. D **44**, 692 (1991).

[15] M. Zhalov, private communication.

[16] W. R. Greenberg and G. A. Miller, Phys. Rev. D **47**, 1865 (1993).

[17] B. C. Clark, in *Relativistic Dynamics and Quark-Nuclear Physics*, edited by M. Johnson and A. Picklesimer (J.

Wiley & Sons, New York, 1986), p. 302.
[18] J. R. Shepard, J. A. McNeil, and S. J. Wallace, Phys. Rev. Lett. **50**, 1443 (1983).
[19] G. Do Dang and N. Van Giai, Phys. Rev. C **30**, 731 (1984).
[20] A. Kohama, K. Yazaki, and R. Seki, Nucl. Phys. **A551**, 687 (1993).
[21] O. Benhar, A. Fabrocini, S. Fantoni, V. R. Pandharipande, and I. Sick, Phys. Rev. Lett. **69**, 881 (1992).
[22] P. Jain and J. P. Ralston, Phys. Rev. D **48**, 1104 (1993).
[23] L. Frankfurt, M. Strikman, and M. Zhalov, Phys. Rev. C (to be published).
[24] A. Picklesimer and J. W. Van Orden, Phys. Rev. C **35**, 266 (1987); **40**, 290 (1989).
[25] C. J. Horowitz and B. D. Serot, Nucl. Phys. **A368**, 503 (1981); C. J. Horowitz, private communication.
[26] C. Itzykson and J. Zuber, *Quantum Field Theory* (McGraw-Hill, New York, 1980).
[27] J. A. McNeil, L. Ray, and S. J. Wallace, Phys. Rev. C **27**, 2123 (1983).
[28] S. J. Wallace, Adv. Nucl. Phys. **12**, 135 (1981).
[29] N. Hoshizaki, Prog. Theor. Phys. **60**, 1796 (1978).
[30] Y. Higuchi and N. Hoshizaki, Prog. Theor. Phys. **62**, 849 (1979).
[31] M. Matsuda, H. Suemitsu, W. Watari, and M. Yonezawa, Prog. Theor. Phys. **66**, 1102 (1981); M. Matsuda, H. Suemitsu, and M. Yonezawa, Phys. Rev. D **33**, 2563 (1986).
[32] See, e.g., R. D. Amado, J. Piekarewicz, D. A. Sparrow, and J. A. McNeil, Phys. Rev. C **28**, 1663 (1983).
[33] W. R. Greenberg, Ph.D. thesis, University of Washington, 1993.
[34] B. K. Jennings and G. A. Miller, Phys. Rev. Lett. **69**, 3619 (1992).
[35] L. Frankfurt, G. A. Miller, and M. Strikman, Phys. Lett. B **304**, 1 (1993). The two-gluon exchange term is $xG(x)$, where G is the gluon structure function. The factor x arises from the vector nature of the nucleon matrix element.
[36] The DWIA results of Refs. [14,16] contain a slight numerical error; the DWIA ratio for ^{12}C using harmonic oscillator wave functions is 0.50 (instead of 0.54) and is 0.54 using Hartree-Fock wave functions.
[37] B. K. Jennings and G. A. Miller, Phys. Lett. B **318**, 7 (1993).
[38] J. V. Noble, Phys. Rev. C **17**, 2151 (1978).
[39] Y. Horikowa, F. Lenz, and N. C. Mukhopadhyay, Phys. Rev. C **22**, 1680 (1980).
[40] B. K. Jennings and B. Z. Kopeliovich, Phys. Rev. Lett. **70**, 3384 (1983).
[41] A. Bianconi, S. Boffi, and D. E. Kharzeev, University of Pavia Report FNT/T-93/45, 1993. Also, University of Pavia Report FNT/T-93/46, 1993.
[42] L. Frankfurt and M. Strikman, Phys. Rep. **76**, 215 (1981).
[43] M. Strikman, private communication.
[44] W. Grein and P. Kroll, Nucl. Phys. **B137**, 173 (1978).
[45] J. Bystricky, F. Lehar, and P. Winternitz, J. Phys. (Paris) **39**, 1 (1978).
[46] D. R. Rust *et al.*, Phys. Lett. **58B**, 114 (1975); R. D. Klem *et al.*, Phys. Rev. D **15**, 602 (1977).
[47] S. L. Kramer *et al.*, Phys. Rev. D **17**, 1709 (1978).